Electrochemistry Communications 111 (2020) 106645

Contents lists available at ScienceDirect

Electrochemistry Communications

journal homepage: www.elsevier.com/locate/elecom

Tubular hollow fibre electrodes for CO_2 reduction made from copper aluminum alloy with drastically increased intrinsic porosity

Daniel Bell[a,1], Deniz Rall[a,b,1], Maren Großeheide[a], Lennart Marx[a], Laura Hülsdünker[a], Matthias Wessling[a,b,*]

[a] RWTH Aachen University, AVT.CVT – Department of Chemical Engineering, Chemical Process Engineering, Forckenbeckstrasse 51, 52074 Aachen, Germany
[b] DWI – Leibniz Institute for Interactive Materials, Forckenbeckstrasse 50, 52074 Aachen, Germany

ARTICLE INFO

Keywords:
CO_2 reduction
Porous metals
Gas diffusion electrode
Tubular hollow fibre
Copper aluminum alloy

ABSTRACT

Electrochemical reduction of CO_2 to higher-order hydrocarbon products offers a significant contribution to the challenge of a circular economy. In the pursuit of better copper metal catalyst, it was early on realized that increasing productivity of copper catalysts systems is reliant on high surface area per volume. Tubular gas diffusion electrodes offer such properties. In this work, we present a methodology to fabricate tubular hollow fibre copper electrodes with drastically increased intrinsic porosity. Our described method utilizes a standard dealloying process of copper aluminium particles to induce an intra-particle nanoporosity. The specific surface area increases from 0.126 $m^2\ g^{-1}$ before dealloying to 6.194 $m^2\ g^{-1}$ after dealloying. In comparison to conventional planar copper electrodes and literature data from conventional copper hollow fibres, the intra-particle porosity leads to a drastically increase in electrochemical activity. Electrochemical measurements reveal increased current densities at low over-potentials in comparison to conventional copper electrodes under identical experimental conditions emphasizing the significant impact of the porosity on the electrode performance. The presented method can be easily transferred to other alloy particles, highlighting its versatility for electrode fabrication.

1. Introduction

Electrochemical reduction of CO_2 has attracted considerable attention as a promising solution for current environmental challenges [1,2]. Existing value chains change through the development of a circular economy by including sustainable sources of raw materials. Capturing CO_2 and subsequent electrochemical reduction to CO and higher-order hydrocarbon product offers a great contribution here [3–5].

Copper is a highly effective catalyst for the electrochemical CO_2 reduction to higher-order hydrocarbons in a sustainable production route of feedstock materials for the chemical industry [6,7]. Catalyst morphology and crystal orientation have a major impact on the selectivity, while the electrochemically active surface area mainly determines the production rate [8,9]. Increased catalyst productivity for the electrochemical CO_2 reduction, is critical to reach industrial scale requirements. Furthermore, an increased electrochemically active surface area per electrode may overcome the limitations that arise when considering the low solubility of CO_2 in aqueous solutions [10]. Although several improvements in the electrode and reactor design e.g. continuous flow cells with gas diffusion electrodes were archived in recent years, the main focus in electrochemical CO_2 reduction research still lies on planar electrodes [11,12].

Recent developments in tubular electrodes offer new possibilities regarding the overall cell design. Porous microtubes made of carbon nanotubes for fuel cell applications and porous titanium hollow fibres have been reported for electrochemical applications [13,14]. Concurrently, the tubular architecture allows direct utilization as (1) a gas diffusor and (2) an electrode. The utilization of such gas diffusion electrodes is a promising way to improve the electrochemical CO_2 reduction as the direct gas supply through the electrode leads to significantly shorter diffusion pathways (50 μm to 50 nm), leading to increased current densities [15].

Tubular hollow fibers made from metallic particles are of great importance, since they offer high stability, a large surface area, easy and cheap production and can be made from various metals depending on the desired application [16]. Copper based hollow fibers have shown

* Corresponding author at: RWTH Aachen University, AVT.CVT – Department of Chemical Engineering, Chemical Process Engineering, Forckenbeckstrasse 51, 52074 Aachen, Germany.
E-mail address: manuscripts.cvt@avt.rwth-aachen.de (M. Wessling).
[1] These authors contributed equally to this work.

https://doi.org/10.1016/j.elecom.2019.106645
Received 11 October 2019; Received in revised form 18 December 2019; Accepted 18 December 2019
Available online 26 December 2019

to be suitable for different electrochemical applications. They are successfully used for the electroforming of metal-organic frameworks in which the hollow fiber acts as a mechanical support and simultaneously as a metal source [17]. Furthermore, Liu et al. demonstrated the successful implementation of copper hollow fibers in membrane bioreactors. It was demonstrated that this kind of membranes outperform conventional polymeric hollow fibers, as the can be used as an electrode during filtration preventing biofouling [18]. In 2016 tubular hollow fibers made from non-porous copper particles were for the first time successfully applied as an electrode for CO_2 reduction [19]. The measurements show a high catalytic activity with low overpotentials for CO_2 reduction emphasizing the advantage of a porous tubular electrode structure with a large three-phase boundary for gas-liquid reactions.

Recent publications utilize a second metal in order to specifically tailor the catalytic activity. Allioux et al. used nickel-copper alloy hollow fibers for the remediation of organic pollutants by electrocatalysis [20]. Furthermore, copper hollow fibers were doped with gold or nickel after the hollow fiber production by electrodeposition in order to tailor the binding energy of intermediates and to decrease the overpotential during CO_2 reduction [21]. All These tubular electrodes contain non-porous particles connected via sintering as building blocks, leading to an inter-particle porosity with large pores [16]. Beside the optimization of the catalyst composition, a further increase in the electrochemically active surface area is a crucial factor for an optimized productivity in CO_2 reduction [9].

The surface area of heterogeneous catalyst particles can be increased either by using smaller- or porous particles. A special catalyst type with a high active surface area are Raney-type catalysts. This catalyst type consist of bimetallic particles (i.e., NiAl, CuAl, and NiCu). In order to activate the catalyst, one component is removed by a dealloying (or selective leaching) process, leading to a porous particle with high surface area and high number of catalytic active centers. For example, this procedure has been utilized to fabricate highly efficient electrocatalyst for methanol oxidation [22] using copper manganese alloy powders. Raney-type catalysts consisting of copper-nickel alloy have been reported for hydrogen production and methane decomposition [23,24].

In the scope of this work, the concept of chemical dealloying is used to prepare metallic hollow fibres with a hierarchical porosity. Copper aluminium alloy particles are utilized as precursor particles for CO_2 reduction. The copper electrodes are produced in a dry-wet spinning procedure. To introduce more porosity into the electrode, copper aluminum alloy micro-particles are dealloyed using hydrochloric acid [25–27] before fibre preparation. As a result of the dealloying process, the aluminum is removed from the particles. This results in a porous copper matrix with a drastically increased surface area. Subsequently, the fibres are tested for their applicability as gas diffusion electrodes in CO_2 reduction experiments.

2. Material and methods

2.1. Copper/aluminum alloy powder and a priori dealloying

For the production of highly porous copper particles, copper aluminum particles (Nanoval, Germany) with a mean particle size of 13µm are utilized as precursor. These particles contain 50 wt% copper and 50 wt% aluminum. For chemical dealloying the precusor particles are treated with 25% hydrochloric acid at room temperature to selectively dissolve the aluminum domains in the particles. The amount of hydrocloric acid is set to four times the stoichiometric ratio needed to dissolve the aluminum. The reaction is completed after five hours when no gas evolution is observed. The dealloyed product is then washed with ultrapure water to remove acid residues and dried over night.

2.2. Spinning of green fibres and thermal post-treatment

In a first step, green copper hollow fibres are produced. Green fibres have the function to set and maintain the shape during the formation process of the metallic monolith during thermal post-treatment. A state-of-the-art hollow fibre spinning line is used for the production of green copper hollow fibres in a non-solvent induced phase separation (NIPS) process. They are produced as reported in our previous work [14] by solving a polymer binder polyethersulfone (PES) in an organic solvent N-Methyl-2-pyrrolidon (NMP) and immersing the metal powder therein. The so-called dope solution is then solidified into a green fibre by a subsequent phase inversion in a water bath. The dope solution is spun through the spinneret to form the tubular shape. All spinnerets used are fabricated through rapid prototyping as reported in our previous work [28]. The fibre is held in place in the water bath by a small guiding wheel and taken out of the water bath at constant speed by a pulling wheel. All green fibres are placed in an additional water baths for proper solvent exchange for at least for 48 h. The dope and aqueous bore fluid compositions as well as the spinning parameter applied are listed in the Supplementary material.

In a second step, the spun green-fibres are post-processed in a thermal treatment step to obtain a solid porous metallic monolithic fibre, as presented in our previous work [14,28]. During thermal treatment the polymer binder of the green-fibre is decomposed and the powder forms sinter connections to build a solid porous matrix at 600°C for 1.5 h. The parameters of the thermal treatment are adapted in accordance with the new material system. The experimental setup and parameters applied are listed in the Supplementary material.

2.3. Electrochemical characterization

Data for linear sweep voltammetry (LSV), electrochemical impedance spectroscopy (EIS), long-term stability tests and polarization curves are collected in a H-cell. A three-electrode setup including a platinized titanium plate as anode, a $Hg/HgSO_4$ reference electrode and the copper hollow fibre as cathode is used. A cation exchange membrane separates anode and cathode compartment, where 0.05 M H_2SO_4 is used as anolyte and 0.5 M $KHCO_3$ as catholyte. Either CO_2 or Ar is flushed through the hollow fibre during the electrochemical experiments for determination of the electrochemical activity of the electrode. Reference experiments are carried out with a non-porous metal copper plate to investigate the influence of catalyst morphology and electrode geometry on the electrochemical activity. As a measure for the electrochemical activity, the respective current densities (quotient of resulting current and geometric surface area of the electrode without considering the intrinsic porosity) are compared. All set potentials are corrected for ohmic resistances obtained by EIS measurements. Further details on the electrochemical measurements and the cell setup are given in the supplementary material.

3. Results & discussion

3.1. Fabrication of tubular hollow fibre electrodes

Metallic copper hollow fibres are prepared via a dry-wet spinning process. Prior to the spinning step, copper aluminum precursor particles are treated with hydrochloric acid to dissolve the aluminum domains in the particles. Fig. 1A and B show the corresponding SEM images of the precursor and the dealloyed particles. The precursor particles are round shaped with a smooth surface. After the dealloying step, the particle size and shape is preserved whereas the morphology changed from a solid particle to a skeletal structure. This fact is an indication for the successful removal of the aluminum domains from the particles, leading to intra-particle porosity.

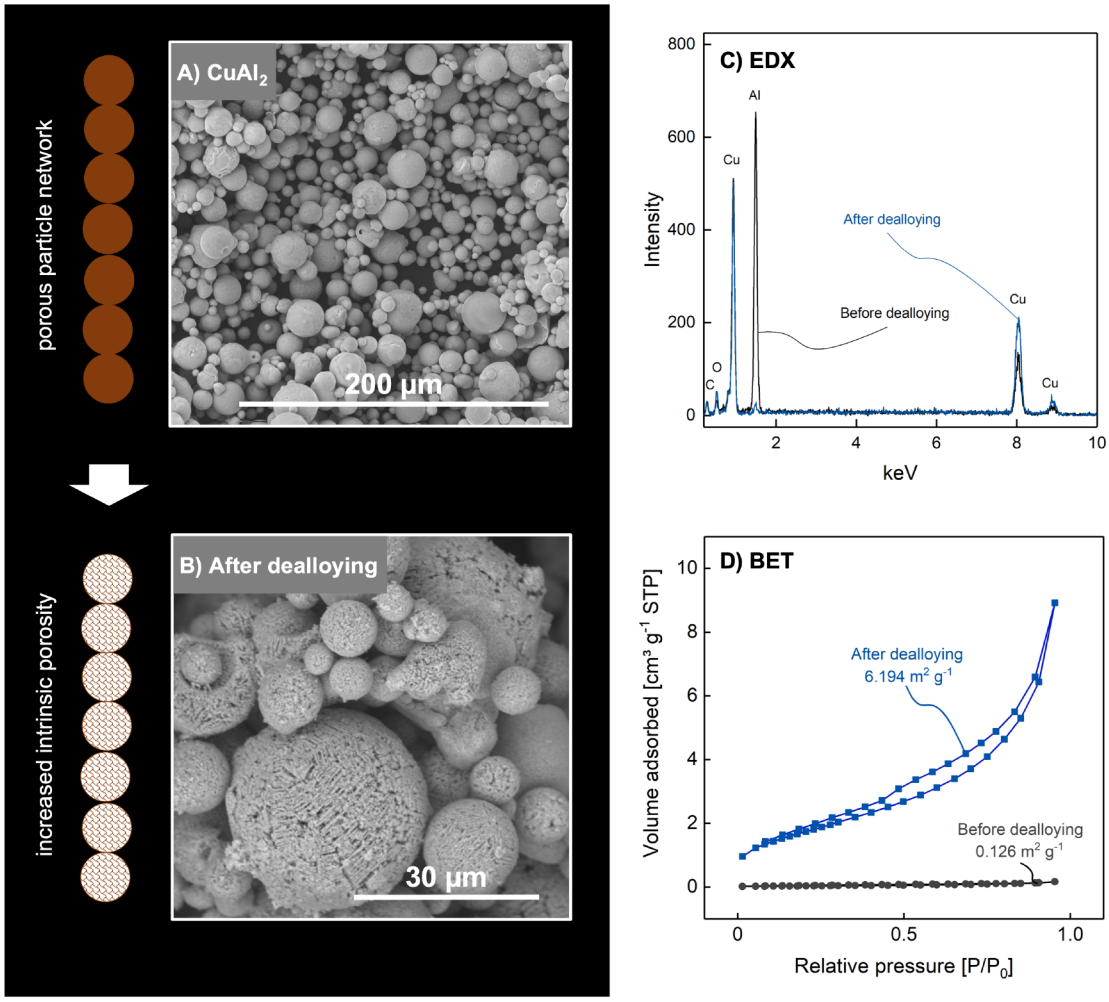

Fig. 1. Schematic illustration of the acidic dealloying process; FeSEM images of the A) untreated $CuAl_2$ powder and B) $CuAl_2$ powder after dealloying procedure showing higher intrinsic porosity. C) EDX spectra of the $CuAl_2$ powder (black) and the leched powder (blue). D) N_2 isotherms at 77K for the reference powder (black) and the dealloyed powder (blue). (For interpretation of the references to colour in this figure legend, the reader is referred to the web version of this article.)

To confirm the dissolution of aluminum, the precursor and the dealloyed particles are analyzed by energy-dispersive X-ray spectroscopy (EDX) (c.f. Fig. 1 C). The results show the successful reduction of the aluminum content from 48 ± 2.01 wt% to 2.5 ± 0.47 wt%. Within the range of accuracy of the EDX measurements, this can be considered a full removal of the aluminum. However, EDX measurements only analyse the first 1–2 µm due to the limited penetration depth [29].

In order to ensure, that aluminum is also dissolved from the core of the particles, we use Inductively Coupled Plasma Emission Spectroscopy (ICP-OES) to analyse the bulk composition of the reference and the dealloyed metal powder. The ICP-OES analyses showed a decrease from 38 wt% to 0.7 wt% showing a successful Al removal within the whole particle. This is in agreement with literature, showing the full Al dissolution from Al-Cu ribbons (20-40 µm thickness) after dealloying in HCl [30].

Chemical dealloying may cause strong oxidation of the material. Therefore, the oxidation of the dealloyed powder is evaluated in comparison to the reference powder by EDX-Analysis. The size of the oxygen peak is not significantly increased after the dealloying process (c.f. Fig. 1C) The quantitative analysis of the spectra displays an oxygen content of 2.52 ± 0.54 wt% before and 2.24 ± 0.14 wt% after the dealloying process. This demonstrated that the applied dealloying process does not lead to strong oxidation, which is in agreement with literature on the dealloying of Zn-Cu and Al-Cu alloys in HCl [31,30].

The non-porous precursor and the dealloyed powder is analyzed by N_2 adsorption/desorption experiments, to evaluate the proposed increased surface area and porosity. Fig. 1 D shows the isotherms for the non-porous precursor (black) and the dealloyed powder (blue). The isotherm of the dealloyed powder shows significant adsorption, whereas nearly no adsorption is detectable with the reference. The Brunauer-Emmett-Teller (BET) surface areas are determined to be 0.126 $m^2\ g^{-1}$ for the non-porous precursor and 6.194 $m^2\ g^{-1}$ for the dealloyed powder indicating an increase in surface area by a factor of 50. This surface area is in the range of other nanoporous copper structures synthesised by acidic dealloying [27].

The porous copper particles are mixed with a polymer (PES) and a solvent (NPM). This mixture is extruded through a spinneret into the coagulation bath. Due to the non-solvent induced phase separation process, the polymer solidifies leading to entrapment of the copper particles into the polymer matrix (cf. Fig. 2A and B). The resulting green fibre has a tubular round structure with a diameter of 4mm and a wall thickness of 350µm (cf. Fig. 2A and E). The fibre wall consist of evenly distributed copper particles embedded into the PES matrix without any visible defects. After thermal treatment, the polymer matrix is decomposed and the copper particles are sintered together (cf. Fig. 2C, D and E), leading to a conductive porous hollow fibre. Induced by the high temperatures during the sintering step, the metal atoms can diffuse and rearrange [32,33], leading to equilibration of the element distribution in the particles, so that there is no significant change in the

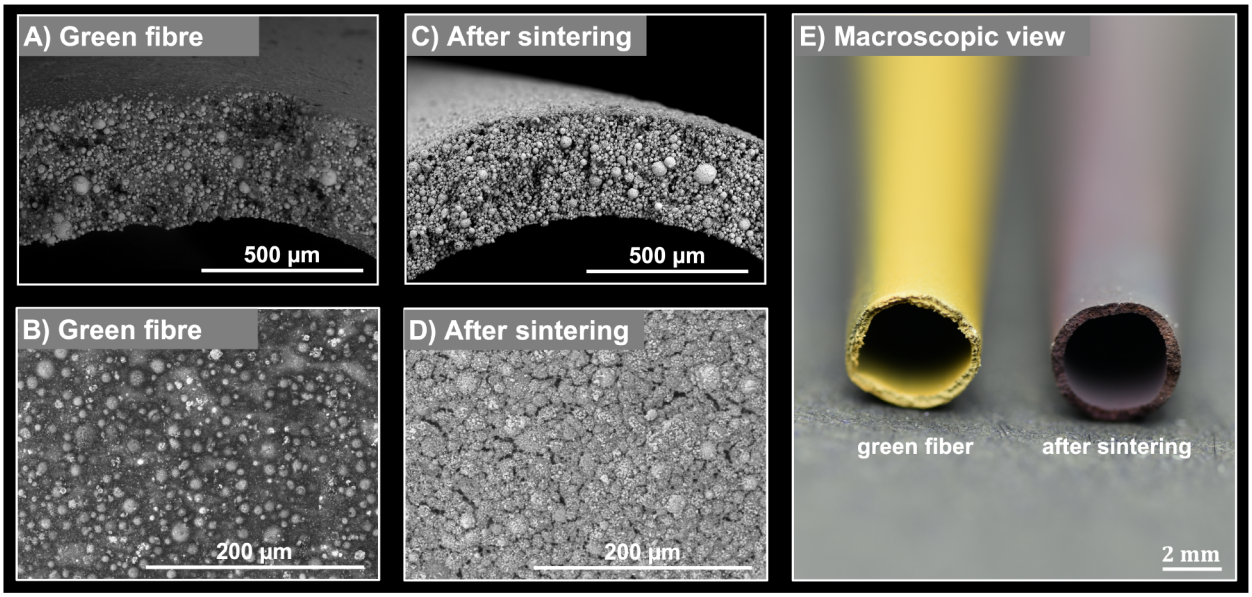

Fig. 2. FeSEM images and macroscopic images of A) and B) the green fibre after dry-wet spinning as cross-section and top view of the fibre at different magnifications. C) and D) show the fibres after thermal post-treatment from the view of the cross-section of the fibre at different magnifications. E) shows the difference between the green fibre and the sintered fibre. After the dealloying procedure the fibre is yellowish. After thermal treatment the fibre shrinks and changes colour. Apart from shrinkage, the fibres structure is maintained. (For interpretation of the references to colour in this figure legend, the reader is referred to the web version of this article.)

catalyst activity afterwards due to eventual migration of aluminum to the surface, since the diffusion at room temperature is very slow. The sintering time and temperature strongly influence the porosity, conductivity and stability of the hollow fibre. On the one hand, longer sintering time at higher temperatures leads to stable fibres with high conductivity. On the other hand, longer sintering time at higher temperatures leads to decreasing porosity. During the sintering step as performed in this study, the intra-particle porosity and the fibre morphology are preserved. Moreover, no voids or defects are detectable. A defect free hollow fibre is desirable with regards to the utilization as a gas diffusion electrode (GDE).

3.2. Electrochemical characterization of tubular hollow fibre electrodes

Electrochemical measurements are performed to analyse the catalytic activity of the produced hollow fibres. In an H-cell setup the hollow fibre is used as the cathode and a gas diffusor at the same time. To evaluate the influence of the porous morphology, a planar copper plate is used as a reference. The current densities of the respective electrodes are plotted with the set potential vs. reversible hydrogen electrode (RHE). The results of the linear sweep voltammetry are shown in Fig. 3A, and long-term stability tests in Fig. 3B. Fig. 3C shows the polarization curves for electrochemical CO_2 reduction with a copper hollow fibre.

Linear sweep voltammetry (LSV) is utilized for comparison with copper hollow fibres with no intra-particle porosity as previously reported in literature [19]. A comparison of LSVs of the full metal copper plate, our highly porous copper hollow fibre, and the copper fibre reported in [19] is shown in Fig. 3 A. The current densities of the copper plate result in near zero values for potentials between 0 V and −0.8 V vs. RHE. Between −0.8 V and −1 V vs. RHE the current densities decrease to about −14 mA cm^{-2}. For potentials between 0 V and −0.4 V vs. RHE the current densities of our porous copper hollow fibre range between −6 mA cm^{-2} and −18 mA cm^{-2}. For the copper plate and the porous copper hollow fibre small peaks at around −0.1 V can be seen. These peaks correspond to the reduction of Cu^{2+} to Cu^0 which takes place at a potential of −0.097 V vs. RHE according to literature [34]. For potentials lower than −0.4 V vs RHE the current density drastically decreases and exceeds current densities of −100 mA cm^{-2}, meaning an up to tenfold increase compared to the copper hollow fibre of [19]. This represents a qualitative measure, since LSV does not account for mass transport limitations in steady state operation. However, when comparing the resulting current density of different electrodes at the same applied potential, an increased current density value indicates higher electrochemical activity of that electrode. We used the same experimental conditions as in [19]: the same electrolyte is used for all compared electrodes and the current density is plotted against the RHE, thereby removing the influence of ohmic losses, pH value and the reference electrode potential from the cell potential. In this case, the electrochemical reactivity is the only parameter left to have an influence on electric current flow. Additionally, it has to be considered that optimization of the cell configuration and the use of more monodisperse copper particles may lead to drastically improved performance.

For the investigation of long-term durability of the electrodes a current density of −16.67 mA cm^{-2} was applied to the electrode for 20 h. Fig. 3 B shows the resulting electrode potential vs. RHE over the time period. After the sintering process freshly manufactured electrodes show a distinct running-in behaviour within the first 2.5 h which then changes into a stationary state. It is assumed that in the running-in process the copper is still electrochemically treated and that the mass transfer of the educts/products settles. After the stationary state of the process has been reached, the potential remains constant. These measurements demonstrate the good long-term stability of the developed porous electrodes.

Finally, polarization curves in Fig. 3 C analyse the current density for a copper plate (black) and a porous copper hollow fibre (blue) during CO_2 and Ar gassing, respectively. The data clearly shows significantly increased current densities when the electrode is exposed to CO_2. In comparison to the copper plate, the hollow fibre electrode shows higher current densities over the whole potential range with a more positive onset potential. These increased current densities already emphasize the improvement of the electrode performance by an increased porosity. It should be highlighted that the increased current density under CO_2 gassing is a strong indication for a high performance of the copper hollow fibers towards CO_2 reduction, since other copper based electrodes show decreased current densities under CO_2 gassing

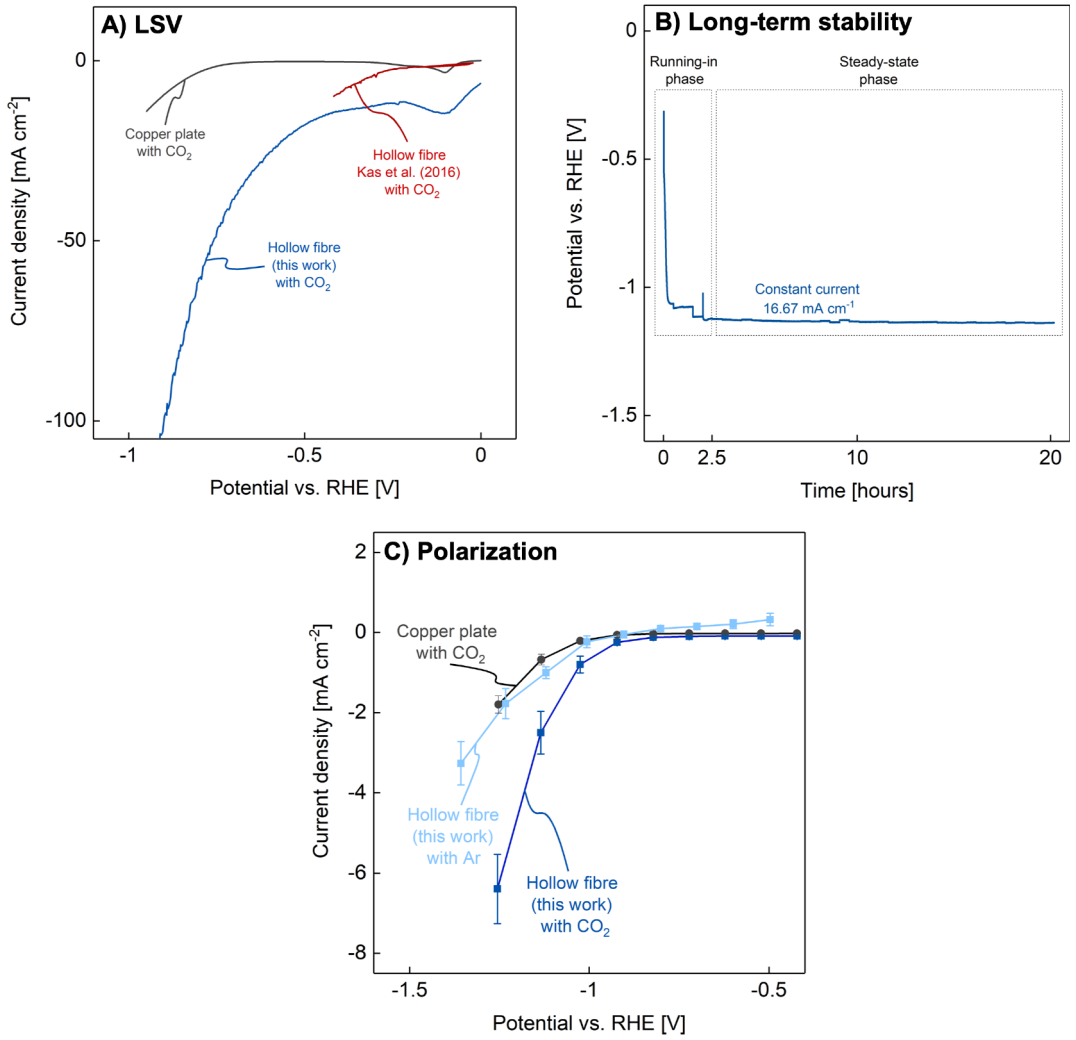

Fig. 3. A) Linear sweep voltammetry curves measured for a copper plate (black) and a porous copper hollow fibre (blue) at a scan rate of 50 mV s^{-1} during CO_2 gassing. The measured data is compared with copper hollow fibres with no intra-particle porosity as previously reported in literature [19] (red). B) Long-term stability test at a current density of 50 mV s^{-1} during CO_2 gassing. C) Polarization curves measured for a copper plate (black) and a porous copper hollow fibre (blue) during CO_2 and Ar gassing, respectively. The current densities are calculated based on the quotient of the resulting current and geometric surface area of the electrode. (For interpretation of the references to colour in this figure legend, the reader is referred to the web version of this article.)

due to strong CO adsorption [35]. This effect has also been reported for non porous copper hollow fiber electrodes [19].

4. Conclusion

This publication demonstrates a new method to introduce a second stage of porosity into metallic hollow fibre electrodes. The selective removal of one metal from a bimetallic particle increases the active surface area.

More precise, in this work, micro-particles made from an alloy consisting of copper and aluminum are dealloyed using hydrochloric acid. The specific surface area increases from 0.126 m^2 g^{-1} before dealloying to 6.194 m^2 g^{-1} after dealloying. The dealloyed micro-particles with increased porosity are fabricated into copper electrodes in a dry-wet spinning process with thermal post treatment. This results in a tubular porous copper matrix with a drastically increased surface area. These tubular electrodes are applicable as gas diffusion electrodes for electrochemical CO_2 reduction.

In comparison to conventional planar copper electrodes and even copper hollow fibres made from non-porous particles, the intra-particle porosity leads to a drastically increased performance with high current densities at low over-potentials. These results demonstrate the significance of the electrode surface for a high electrode activity.

The presented method can be easily adapted to other alloy particles. Significantly improved current densities are achieved simply by an adaptable pretreatment of the precursor. Hollow fibre electrodes made from porous particles by an versatile dealloying process may be a step towards new electrodes for electrochemical processes with a high productivity. Furthermore, there is still a lot of potential for improvement of the electrode performance by optimizing the cell design and changing the precursor particle properties e.g. using smaller monodisperse particles. Another very important measure for the functionality of the electrodes is the faradaic efficiency of the products. In further research the product spectrum and tubular electrode modules have to be evaluated.

CRediT authorship contribution statement

Daniel Bell: Conceptualization, Methodology, Investigation, Writing - original draft, Visualization, Writing - review & editing. **Deniz Rall:** Conceptualization, Methodology, Investigation, Writing - original draft, Visualization, Writing - review & editing. **Maren Großeheide:** Methodology, Investigation, Writing - original draft, Visualization, Writing - review & editing. **Lennart Marx:** Investigation. **Laura**

Hülsdünker: Investigation. **Matthias Wessling:** Supervision, Project administration, Funding acquisition, Conceptualization, Writing - review & editing.

Declaration of Competing Interest

The authors declare that they have no known competing financial interests or personal relationships that could have appeared to influence the work reported in this paper.

Acknowledgements

M.W. acknowledges the support through the Gottfried Wilhelm Leibniz award; This project has received funding from the European Research Council (ERC) under the grant agreement No. 694946 and by the Deutsche Forschungsgemeinschaft (DFG, German Research Foundation) under Germany's Excellence Strategy – Exzellenzcluster 2186 'The Fuel Science Center' ID: 390919832.

Appendix A. Supplementary data

Supplementary data associated with this article can be found, in the online version, athttps://doi.org/10.1016/j.elecom.2019.106645.

References

[1] T. Gasser, C. Guivarch, K. Tachiiri, C. Jones, P. Ciais, Negative emissions physically needed to keep global warming below 2C, Nat. Commun. 6 (2015) 7958.
[2] J.-P. Jones, G.S. Prakash, G.A. Olah, Electrochemical CO_2 reduction: recent advances and current trends, Isr. J. Chem. 54 (10) (2014) 1451–1466.
[3] K.P. Kuhl, E.R. Cave, D.N. Abram, T.F. Jaramillo, New insights into the electrochemical reduction of carbon dioxide on metallic copper surfaces, Energy Environ. Sci. 5 (5) (2012) 7050–7059.
[4] M. Aresta, A. Dibenedetto, A. Angelini, Catalysis for the valorization of exhaust carbon: from CO_2 to chemicals, materials, and fuels. technological use of CO_2, Chem. Rev. 114 (3) (2013) 1709–1742.
[5] M. Jouny, W. Luc, F. Jiao, High-rate electroreduction of carbon monoxide to multicarbon products, Nat. Catal. 1 (10) (2018) 748.
[6] Y.I. Hori, Electrochemical CO_2 reduction on metal electrodes, Modern Aspects of Electrochemistry, Springer, 2008, pp. 89–189.
[7] F.S. Roberts, K.P. Kuhl, A. Nilsson, High selectivity for ethylene from carbon dioxide reduction over copper nanocube electrocatalysts, Angew. Chem. Int. Ed. 54 (17) (2015) 5179–5182.
[8] D. Raciti, C. Wang, Recent advances in CO_2 reduction electrocatalysis on copper, ACS Energy Lett. 3 (7) (2018) 1545–1556.
[9] E.L. Clark, J. Resasco, A. Landers, J. Lin, L.-T. Chung, A. Walton, C. Hahn, T.F. Jaramillo, A.T. Bell, Standards and protocols for data acquisition and reporting for studies of the electrochemical reduction of carbon dioxide, ACS Catal. 8 (7) (2018) 6560–6570.
[10] R.M. Enick, S.M. Klara, $_2$ solubility in water and brine under reservoir conditions, Chem. Eng. Commun. 90 (1) (1990) 23–33.
[11] F. Bidault, D. Brett, P. Middleton, N. Brandon, Review of gas diffusion cathodes for alkaline fuel cells, J. Power Sources 187 (1) (2009) 39–48.
[12] J.-B. Vennekoetter, R. Sengpiel, M. Wessling, Beyond the catalyst: how electrode and reactor design determine the product spectrum during electrochemical CO_2 reduction, Chem. Eng. J. 364 (2019) 89–101.
[13] Y. Gendel, O. David, M. Wessling, Microtubes made of carbon nanotubes, Carbon 68 (2014) 818–820.
[14] O. David, Y. Gendel, M. Wessling, Tubular macro-porous titanium membranes, J. Membr. Sci. 461 (2014) 139–145.
[15] T. Burdyny, W.A. Smith, $_2$ reduction on gas-diffusion electrodes and why catalytic performance must be assessed at commercially-relevant conditions, Energy Environ. Sci. 12 (5) (2019) 1442–1453.
[16] B. Zhu, M. Duke, L. Dumée, A. Merenda, E. des Ligneris, L. Kong, P. Hodgson, S. Gray, Short review on porous metal membranes-fabrication, commercial products, and applications, Membranes 8 (3) (2018) 83.
[17] Ö. H. Demirel, T. Rijnaarts, P. De Wit, J.A. Wood, N.E. Benes, Electroforming of a metal-organic framework on porous copper hollow fibers, J. Mater. Chem. A.
[18] D. Liu, X. Chen, B. Bian, Z. Lai, Y. Situ, Dual-function conductive copper hollow fibers for microfiltration and anti-biofouling in electrochemical membrane bioreactors, Front. Chem. 6 (2018) 445.
[19] R. Kas, K.K. Hummadi, R. Kortlever, P. De Wit, A. Milbrat, M.W. Luiten-Olieman, N.E. Benes, M.T. Koper, G. Mul, Three-dimensional porous hollow fibre copper electrodes for efficient and high-rate electrochemical carbon dioxide reduction, Nat. Commun. 7 (2016) 10748.
[20] F.-M. Allioux, O. David, A. Merenda, J.W. Maina, M.E. Benavides, A.P. Tanaka, L.F. Dumée, Catalytic nickel and nickel–copper alloy hollow-fiber membranes for the remediation of organic pollutants by electrocatalysis, J. Mater. Chem. A 6 (16) (2018) 6904–6915.
[21] I. Merino-Garcia, J. Albo, P. Krzywda, G. Mul, A. Irabien, Bimetallic Cu-based hollow fibre electrodes for CO_2 electroreduction, Catal. Today (2019), https://doi.org/10.1016/j.cattod.2019.03.025 (in press).
[22] Y. Zhang, X. Sun, N. Nomura, T. Fujita, Hierarchical nanoporous copper architectures via 3D printing technique for highly efficient catalysts, Small 1805432 (2019).
[23] A. Cunha, J. Órfão, J. Figueiredo, Catalytic decomposition of methane on Raney-type catalysts, Appl. Catal. A: Gen. 348 (1) (2008) 103–112.
[24] A. Cunha, J. Órfão, J. Figueiredo, Methane decomposition on Ni–Cu alloyed Raney-type catalysts, Int. J. Hydrogen Energy 34 (11) (2009) 4763–4772.
[25] J. Friedrich, D. Young, M. Wainwright, Caustic leaching of Al-Cu-Zn alloys to produce Raney catalysts II. leaching kinetics, J. Electrochem. Soc. 128 (9) (1981) 1845–1850.
[26] J. Friedrich, D. Young, M. Wainwright, Caustic leaching of Al-Cu-Zn alloys to produce Raney catalysts I. morphological development, J. Electrochem. Soc. 128 (9) (1981) 1840–1844.
[27] W. Liu, L. Chen, J. Yan, N. Li, S. Shi, S. Zhang, Dealloying solution dependence of fabrication, microstructure and porosity of hierarchical structured nanoporous copper ribbons, Corros. Sci. 94 (2015) 114–121.
[28] T. Luelf, D. Rall, D. Wypysek, M. Wiese, T. Femmer, C. Bremer, J.U. Michaelis, M. Wessling, 3D-printed rotating spinnerets create membranes with a twist, J. Membr. Sci. 555 (2018) 7–19.
[29] J. Goldstein, Scanning Electron Microscopy and X-Ray Microanalysis: A Text for Biologists, Materials Scientists, and Geologists, Plenum Publishing Corporation, 1992.
[30] W. Liu, S. Zhang, N. Li, J. Zheng, Y. Xing, Microstructure evolution of monolithic nanoporous copper from dual-phase Al 35 atom% Cu alloy, J. Electrochem. Soc. 157 (12) (2010) D666–D670.
[31] B. Hecker, C. Dosche, M. Oezaslan, Ligament evolution in nanoporous Cu films prepared by dealloying, J. Phys. Chem. C 122 (46) (2018) 26378–26384.
[32] J.P. Bergmann, F. Petzoldt, R. Schürer, S. Schneider, Solid-state welding of aluminum to copper-case studies, Welding World 57 (4) (2013) 541–550.
[33] X. Peng, R. Wuhrer, G. Heness, W. Yeung, On the interface development and fracture behaviour of roll bonded copper/aluminium metal laminates, J. Mater. Sci. 34 (9) (1999) 2029–2038.
[34] A.J. Bard, L.R. Faulkner, J. Leddy, C.G. Zoski, Electrochemical methods: fundamentals and applications vol. 2, John Wiley and Sons Inc, New York, USA, 1980.
[35] Y.-J. Zhang, V. Sethuraman, R. Michalsky, A.A. Peterson, Competition between CO_2 reduction and H_2 evolution on transition-metal electrocatalysts, ACS Catal. 4 (10) (2014) 3742–3748.